symmetry

MDPI

Article

Anatomical Considerations and Study of the Fractal Dimension around the Posterior Superior Alveolar Artery

Yolanda Guerrero-Sánchez [1,*,†], Francisco José Gómez García [1,†], Manuel Fernández-Martínez [2,†] and Blanca Pallarés Martínez [1,†] and Pia López-Jornet [2]

[1] Department of Dermatology, Stomatology, Radiology and Physical Medicine, Morales Meseguer General Universitary Hospital, Avda. Marqués de los Vélez, 30008 Murcia, Spain; fjgomez@um.es (F.J.G.G.); blanca.pallaresmartinez@gmail.com (B.P.M.)

[2] University Centre of Defence at the Spanish Air Force Academy, MDE-UPCT, Santiago de la Ribera, 30720 Murcia, Spain; manuel.fernandez-martinez@cud.upct.es (M.F.-M.); majornet@um.es (P.L.-J.)

* Correspondence: yolanda.guerreros@um.es

† These authors contributed equally to this work.

Received: 31 May 2020; Accepted: 13 July 2020; Published: 16 July 2020

Abstract: The Posterior Superior Alveolar Artery (PSAA) provides vascular support to molars, gingiva, and maxillary sinus. A tear of the PSAA may cause profuse hemorrhages which may lead to complications at a surgical level. As such, it becomes crucial to anatomically analyse several features regarding the PSAA as well as the area surrounding it. In this paper, we are particularly interested in the study of the complexity of the periodontal tissue structure which appears close to the location of the PSAA. A total amount of 400 cone beam computed tomography (CBCT) scans (two per subject) were performed to explore the presence of the PSAA, the thickness of the Schneider's membrane, and the existence of septa. Several parameters were evaluated including the location of the artery in the maxillary sinus, the distance from the PSAA to the alveolar ridge, the thickness of the membrane, the diameter of the cavities produced by the septa, and the fractal dimension of the trabecular tissue that surrounds the PSAA. They were found strong linear relationships between Distal and Central Measures (a Pearson's $R^2 = 0.9952$), Mesial and Central Measures ($R^2 = 0.9950$), and Distal and Mesial Measure ($R^2 = 0.997$). We hypothesised that the loss of dental pieces would imply a distinct complexity of the trabecular tissue structure surrounding the PSAA. In this way, a p-value equal to 0.001 was provided by the Mann-Whitney test, which supports our hypothesis. Furthermore, the mean of the fractal dimensions of the group of edentulous patients (equal to 1.56) was found to be lower than the one of the group of non-edentulous patients (equal to 1.61) with small standard deviations in both cases. Our study suggests that accurate calculations of the fractal dimension combined with the use of CBCT do provide valuable information regarding the area that surrounds the PSAA.

Keywords: maxillary sinus; posterior superior alveolar artery (PSAA); Schneider's membrane; cone beam computed tomography (CBCT); fractal dimension

1. Introduction

The maxillary sinus is an anatomical structure of vital importance which is located in the bone maxillary. Such a gap of air fills most of the upper jaw with its bone margins being usually symmetric and clearly defined [1]. It is the largest of the paranasal sinuses and is originated from a small epithelial diverticulum located in the middle nasal meatus of the nostrils. Its development commences at the first months of gestation at a very slow rate.

Such an anatomical structure is closely related to dental activity and may be affected by several pathologies concerning the stomatologic system including endodontic, periodontal, or cyst infectious processes. It can also be the origin of other pathologies such as retentive phenomena mucous and allergic phenomena [2–6], among others. Maxillary sinus pathologies may occur when the mucosa is altered by distinct causes such as trauma, infections of dental origin, osteitis, cellulite, or iatrogenic including exodontics, endodontic treatments, or placement of osseointegrated implants [7].

In the field of dentistry and maxillofacial surgery, acquiring knowledge regarding the anatomy of the maxillary sinus and analysing their relationships with other anatomical structures becomes crucial to properly perform surgical interventions such as implant placements or sinus lifts. In fact, the latter has become a usual technique with a high rate of success, thus providing an increase in the bone mass of the alveolar crest for subsequent implant placements [8,9]. Nevertheless, several complications may appear during the implementation of that technique. In this way, the main difficulty concerning that intervention consists of the rupture of the Schneider's membrane, thus following the rupture of the posterior superior alveolar artery (PSAA, in the sequel), which in turn, is responsible for irrigating part of the sinus structure [8]. Moreover, there exist anatomical variations from some subjects to others in regard to the maxillary sinus. They include the likely appearance of partitions in the maxillary sinus that may drill the membrane depending on their locations [9]. To avoid these kinds of complications, a rigorous preoperative study concerning such structures becomes crucial to achieve the success of the intervention. Hopefully, the digital technology has brought to dentistry several advances, both in the preoperative (scanners) and surgical (computer assisted implantology) fields [10]. In fact, the development of imaging techniques such as cone beam computed tomography (CBCT in the sequel) has allowed a proper display of such structures [11], thus being consolidated as an appropriate resource to extract valuable information from high resolution images [12,13].

The maxillary artery is one of the terminal branches of the external carotid, which is split into five ramifications in the pterygopalatine fossa, i.e., vidian artery, pterygopalatine, sphenopalatine, suborbital, alveolar, and descending palatine (cf. Figure 1). From such branches, both the PSAA and the infraorbital artery manage the vascular supply of the lateral wall of the sinus and the Schneider's membrane [14–16]. They emit intraosseous and extraosseous branches and form anastomosis around the maxillary sinus. The PSAA is divided, in turn, into two branches, one extraosseous, which irrigates the periosteum and the buccal vestibule, molars, and premolars, and the other intraosseous, which travels through the lateral wall of the sinus.

The infraorbital artery together with the nerve run along the upper wall of the antrum inside the sinus mucosa, and radiate the superior, middle, and anterior alveolar arteries before leaving the skull. One of these branches performs an anastomosis with the intraosseous branch of the PSAA [14]. From that artery, known as the antral alveolar artery, several vascular branches supply the mucous membrane of the maxillary sinus, the periodic tissue, and the anterolateral wall of the maxillary sinus [11].

It is worth mentioning that the intraosseous branch of the PSAA generally describes a straight or unshaped course within the lateral wall of the sinus, forming a concave arch whose closest point to the bone crest is near to the first molar [15]. The enlargement of the maxillary sinus with aging, the resorption of the alveolar crest, and surgical procedures performed in this area are associated with an increased risk of damagecite [15]. Indeed, the accidental rupture of that anastomosis is considered to be the second most frequent intraoperative complication [8].

The anatomical features of such vessels are especially relevant in dental implantology as well as in other oral surgery procedures. The maxillary sinus floor elevation before placement of the dental implant could be carried out by a crestal approach or side. The latter requires access to the maxillary sinus throughout a lateral window, and involves the risk of damaging the blood vessels that are present in the area, usually the PSAA. In fact, from the 10% to the 30% of the cases, the PSAA appears in the area where the side window is created for lifting techniques of the sinus floor. Thus, it becomes crucial

to know the anatomical location of such vessels before initiating any intervention that may present a risk of damage [15,17].

The maximum diameter they can reach is 3.0 mm [17]. However, a CBCT approach does not allow showing arteries with diameters less than 0.5 mm. Hence, small diameter PSAAs may not appear in the CBCT scanners. The same issue arises for those alveolar antral arteries whose location is subperiosteal with respect to the Schneider's membrane, thus not being found in the bone [1]. When that complication occurs and either the anastomosis is broken or the PSAA is damaged, the visibility is reduced and the possibility of a perforation of the Schneider's membrane exists. The management of that complication turns out to be difficult when the diameter of the PSAA is large, contrary to the case of PSAAs that are smaller than 1 mm in diameter, that could be successfully managed since there is no complicated bleeding in the case of injury. Therefore, in the CBCT-based studies, a threshold measure of 1 mm is usually set to measure the PSAA diameter [17].

Following the above, it results of great importance to carry out a rigorous preoperative study to control and identify the anatomical features of the PSAA and the area surrounding it in order to avoid complications that could be derived. In fact, both the presence and the path of the artery must be inspected, for instance, to avoid iatrogenic damage during the procedure of maxillary sinus elevation [17,18].

As such, the main goal in this paper was to analyze various anatomical features concerning the PSAA. Furthermore, some specific objectives of this study are stated next.

- To explore the location of the PSAA and its bifurcations.
- To analise the maxillary sinus and its relationships with bordering dental pieces.
- To identify some anatomical variations concerning the Schneider's membrane.
- To analyze the presence and features of the septa of the maxillary sinus.
- To explore the density of the trabecular tissue located in the area that surrounds the PSAA.

Accordingly, in this paper, they were analyzed a total amount of 400 CBCT scans (two per subject) to explore the presence of the PSAA, the thickness of the Schneider's membrane, and the existence of septa. Several parameters were evaluated including the location of the PSAA in the maxillary sinus, the distance from the PSAA to the alveolar ridge, the thickness of the membrane, the diameter of the cavities produced by the septa, and the fractal dimension values of the trabecular tissue that surrounds the PSAA. Regarding the latter, we were particularly focused on exploring the complexity of the periodontal tissue structure which appears close to the location of the PSAA. In fact, the fractal dimension is a key tool used in odontology to assess the quality of trabecular tissues and how they evolve with aging. It is noteworthy that our fractal dimension calculations were carried out by an accurate procedure described in Section 2 (cf. [12,13,19]).

Regarding the bone structure density of the trabecular tissue in the area that surrounds the PSAA, we hypothesised that the loss of dental pieces would imply a different (probably lower) complexity of that bone structure. The 200 people who participated in this study were assigned to one of the following two groups. The non-edentulous group of patients, $\mathcal{G}_{\mathrm{NE}}$, consisted of 63 subjects, whereas 137 people were assigned to $\mathcal{G}_{\mathrm{E}}$, the group of partially or totally edentulous patients. According to our hypothesis, distinct values of the fractal dimensions of the trabecular tissues located in the area surrounding the PSAA would be expected for those patients assigned to the group $\mathcal{G}_{\mathrm{E}}$. To verify it, the following test of hypotheses was posed:

$$\begin{aligned} \mathcal{H}_0 &: \mu_{\mathrm{NE}} = \mu_{\mathrm{E}} \\ \mathcal{H}_1 &: \mu_{\mathrm{NE}} \neq \mu_{\mathrm{E}}, \end{aligned} \tag{1}$$

where μ_{NE} denotes the mean (resp., the median) of the fractal dimensions of the binary CBCTs (from the original high quality CBCTs) of the group of subjects in the group of non-edentulous subjects, and μ_{E} refers to the mean (resp., the median) of the fractal dimensions of the binary CBCTs of the group of (partially or totally) edentulous patients assigned to the group $\mathcal{G}_{\mathrm{E}}$.

In this paper, we show that high quality CBCTs combined with accurate fractal dimension calculations do provide valuable information in regard to the area that surrounds the PSAA.

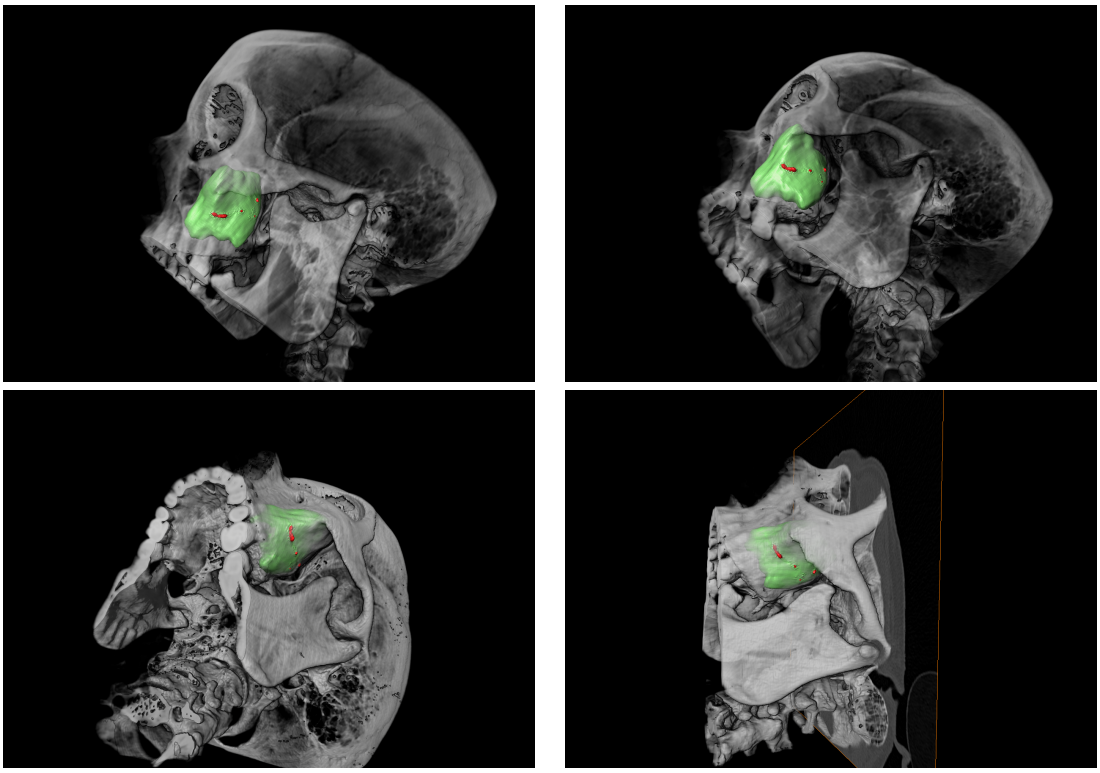

Figure 1. 3D volumetric reconstruction of the left maxillary sinus and superficial path of the PSAA (marked in red) as provided by the software AMIRA® (Thermo Fisher Scientific, Berlin, Germany).

2. Material and Methods

This is a longitudinal, non cross-sectional, and retrospective clinical study for which we consecutively selected a sample of 200 subjects from the University Dental Clinic at the Morales Meseguer Hospital (Murcia, Spain).

It is worth pointing out that such a study was approved by the Bioethics Committee of the University of Murcia (ID: 1902/2018), and conducted in the University Dental Clinic at the Morales Meseguer Hospital (Murcia, Spain). All the involved participants provided their informed consent in writing. In addition, they had required diagnosis and/or planning for a craniofacial pathology treatment.

The process of image acquisition lasted 3 years. During that time, the University Dental Clinic at the Morales Meseguer Hospital (Murcia, Spain) provided us access to its archive. Thus, a collection of CBCTs from 100 subjects fulfilling the next inclusion criteria was involved in our study.

- To be over 18 years old.
- To have been undergone a radiological test according to the needs for treatment.

Moreover, it was included a set of CBCTs from 100 new subjects who, in addition, did not satisfy any of the following exclusion criteria:

- To be a children or a pregnant woman.
- To have taken any medication that could affect their bone density.
- To have suffered any pathology directly affecting bones.

Then such images were thorough analyzed according to the systematic methodology described in this section.

A pair of CBCT high resolution images was chosen (one scanner per side) for each of the 200 participants in this study, thus leading to a collection of 400 CBCTs of maxillary sinuses. Definitely, those CBCTs with a poor quality or including artefacts were excluded from the study.

The image acquisition process was carried out by a same examiner with the aim that all the CBCTs were treated with a same action protocol. It is worth mentioning that all the CBCT images were analyzed by Romexis 2.5.1® (Planmeca Oy, Helsinki, Finland), a powerful software that enables several approaches of each patient's scanner. On the other hand, all the numeric results provided in Section 3 were obtained by Mathematica 12.0® (Champaign, IL, USA).

Firstly, each CBCT was classified according to the sex of the patient and the type of edentulous to be treated. Regarding the latter, each CBCT was classified according to the (qualitative) attribute TED (Type of EDentulous), which distinguished between three kinds of subjects:

- those who had lost all their teeth (type I: totally edentulous).
- those who had lost some dental pieces (type II: partially edentulous), and
- those who kept all their teeth (type III: non-edentulous).

Our analyses commenced from the left sinus in order to establish a sequence of steps to facilitate the data collection. Afterwards, it was registered the presence or absence of the PSAA to the height of the superior molars. As such, the (qualitative) variable PAA (Presence of Alveolar Artery) allowed to distinguish between two categories, namely,

- type I, if no alveolar artery was found in the corresponding CBCT.
- Type II, provided that some alveolar artery appeared in the image.

Going beyond, for all those subjects whose alveolar arteries were found, the (qualitative) attribute AAL (Alveolar Artery Location), which distinguished among five categories, was defined according to a thorough review of the literature concerning the PSAA (cf., e.g., [16]). The levels of such a variable were as follows.

- Location I: when there is absence of alveolar artery.
- Location II (superficial): if the alveolar artery is located at the external face of the sinus wall.
- Location III (intraosseous): when the alveolar artery go across the sinus wall.
- Location IV (intrasinusal): if the alveolar artery is located at the inner face of the sinus wall.
- Location V (bifurcated): when the alveolar artery appears divided into two paths.

It is worth mentioning that each subject in the type II category of PAA) was measured the Distance from the alveolar Artery to the Bone crest (in millimetres, mm). That quantitative variable was named DAB accordingly.

On the other hand, the presence of a pathological Schneider's membrane was also analyzed. In this way, a normal thickness of such a membrane varies from 0.3 to 0.8 mm. As such, a Schneider's membrane is classified as pathological when its thickness exceeds 0.8 mm. Following the latter, the qualitative variable PSM (Presence of a pathological Schneider's Membrane) allowed to distinguish between two categories, i.e., the one consisting of those subjects who presented a pathological Schneider's membrane (type I), and another one consisting of those people who did not (type II). Additionally, every patient assigned to the type I category of PSM was calculated each of the next three quantities, namely, Distal MEasure (DME), Central MEasure (CME), and Mesial MEasure (MME).

Also, the presence of septa, that divide the sinus in more than one compartment, was explored. In this way, the (qualitative) variable NSE (Number of SEpta) allowed to detect the presence of septa according to their orientation through one of the next three levels.

- Type I: absence of septa.
- Type II: existence of mediolateral vertical septa (when they are divided from right to left).
- Type III: existence of anteroposterior vertical septa.

Going beyond, for all those people with presence of septa (i.e., assigned to either type II or type III classes of NSE), two additional quantities were calculated, namely, Diameter of the Anterior Hole (DAH) and Diameter of the Posterior Hole (DPH), as well.

In this paper, a special attention has been paid to explore the complexity of the structure of the trabecular tissue located in the area that surrounds the PSAA. With this aim, a novel algorithm especially designed to accurately calculate the fractal dimension of binary CBCTs was applied (cf. [12,13]). With this aim, all the 400 CBCTs of maxillary sinuses were assigned to one of two subgroups. Specifically, 126 CBCTs (from 63 non-edentulous patients) were assigned to the subgroup $\mathcal{G}_{\mathrm{NE}}$, whereas another 274 CBCTs (from 137 subjects being partially or totally edentulous) were assigned to the subgroup $\mathcal{G}_{\mathrm{E}}$.

Each CBCT scanner was firstly transformed into a binary image (called binary CBCT, hereafter) by assigning "zeros" to all those pixels in the original CBCT being under a certain threshold of colour and "ones" on the contrary. The calculations involving the fractal dimensions of the binary CBCTs were performed by means of the following expression (cf. [12,13,20]):

$$\dim(F) = 2 \cdot \lim_{\delta \to 0} \frac{\log N_\delta(\alpha^{-1}(F))}{-\log \delta},$$

where for each $n \in \mathbb{N}$ (in the computational practice, for a finite range of natural values of n), $\delta (= 2^{-n})$ is the scale that was chosen to explore the irregularities of the set F (in this case, the set consisting of all the pixels in the binary CBCT being analyzed), $N_\delta(\alpha^{-1}(F))$ quantifies the number of $\delta-$cubes that meet the set $\alpha^{-1}(F)$, a $\delta-$cube in $[0,1] \times [0,1] \subset \mathbb{R}^2$ is a set of the form $[k_1\,\delta, (k_1+1)\,\delta] \times [k_2\,\delta, (k_2+1)\,\delta] : k_1, k_2 = 0, 1, \ldots, 2^n - 1$, and $\alpha^{-1}(F)$ denotes the preimage of the set F by a function $\alpha : [0,1] \to [0,1] \times [0,1]$ (with F, the binary CBCT, having been rescaled previously to the unit square, $[0,1] \times [0,1]$). For additional details concerning the theoretical support underlying this approach, we refer the reader to Section 3.11 of [21]. Also, the construction of the function α was illustrated in detail in [12] Example 2.8 according to [12] Theorem 2.7. Anyway, a Hilbert type plane-filling curve could be easily defined by levels for fractal dimension calculation purposes, which constitutes an appropriate choice for α.

The same approach was applied in regard to the right maxillary sinus, thus completing our CBCT collection.

3. Results

Regarding the 200 participants in this study whose data were analyzed, it was calculated a mean age equal to 51.54 years old with a standard deviation of 8.53 years. Specifically, the female group consisted of 119 people, whereas the remaining 40.5% of the sample (i.e., 81 subjects) were men. As such, a ratio of 1.47 women per men was found. Moreover, it is worth pointing out that 102 people (51%) in the sample did not smoke.

The size of the levels of each qualitative attribute involved in this study appears in Table 1.

On the other hand, Table 2 collects the summary statistics (means and standard deviations) for each quantitative attribute analyzed in this article. It also displays the number of subjects they were calculated for (denoted by n therein). It is worth noting that, apart from DIM, such quantities were not quantified for all the participants in the study. In fact, for instance, DAB depends on the presence of the alveolar artery (i.e., all the subjects assigned to the type II category of PAA); DME, CME, and MME were calculated for all the patients in the type I class of PSM; and DAH and DPH were calculated only for those subjects who were detected some septa (i.e., the patients assigned to either the type II level or the type III category of NSE).

Table 1. Distribution of subjects by five (qualitative) attributes and several levels, where the ratios were calculated with respect to all the 200 participants in this study. Acronyms: TED, Type of EDentulous; PAA, Presence of Alveolar Artery; AAL, Alveolar Artery Location; PSM, Presence of a pathological Schneider's Membrane; NSE, Number of SEpta.

Attribute	No. of Levels	Size of Levels		Ratio (%)
TED	3	**type I**	66	33
		type II	99	49.5
		type III	35	17.5
PAA	2	**type I**	142	71
		type II	58	29
AAL	5	**location I**	142	71
		location II	5	2.5
		location III	23	11.5
		location IV	29	14.5
		location V	1	0.5
PSM	2	**type I**	76	38
		type II	124	62
NSE	3	**type I**	162	81
		type II	28	14
		type III	10	5

Table 2. Summary statistics for all the quantitative variables involved in this study, where n denotes the number of participants they were calculated for. All such quantities (with the exception of DIM) are expressed in mm. Ratio was calculated with respect to the 200 people involved in the study. DIM was calculated for all the 200 participants, thus involving 400 CBCTs (one image per side). Acronyms: DAB, Distance from the alveolar Artery to the Bone crest; DME, Distal MEasure; CME, Central MEasure; MME, Mesial MEasure; DAH, Diameter of the Anterior Hole; DPH, Diameter of the Posterior Hole; DIM, fractal DIMension.

Attribute	n	ratio (%)	Mean $\pm$ Std.
DAB	58	29	16.90 ± 3.59
DME	76	38	17.41 ± 34.21
CME	76	38	19.25 ± 33.57
MME	76	38	17.78 ± 34.93
DAH	38	19	12.57 ± 4.64
DPH	38	19	9.83 ± 3.99
DIM	200	100	1.57 ± 0.16

It is worth pointing out that several pairs of (quantitative) attributes were found to exhibit a strong linear relationship. In this way, it was found that a Pearson's R^2 coefficient equal to 0.9952 concerning the variables DME and CME. A R^2 coefficient equal to 0.9950 was obtained when comparing CME and MME attributes. Hence, a strong linear correlation between DME and MME was expected by transitivity. In fact, a linear correlation coefficient equal to 0.997 was found in regard to DME and MME.

Table 3 summarizes the ratios as well as the number of participants in the study who were found some kind of septa. Notice that there were found 74 people (18.50% of the sample) with some type II (mediolateral vertical) or type III (anteroposterior vertical) septa. It is worth noting that almost the half of all the partially edentulous patients (35 people) presented some septa of type II.

Regarding the fractal dimension of the 400 high resolution scanners, a mean fractal dimension equal to 1.57 (resp., a median equal to 1.57) and a standard deviation equal to 0.16 (a variance of 0.03) were obtained. In particular, the binary CBCTs from the subjects assigned to the group $\mathcal{G}_{\mathrm{E}}$ (edentulous patients) were calculated a mean fractal dimension equal to 1.56 (resp., a median equal to 1.56) together with a standard deviation of 0.12 (a variance of 0.014). On the other hand, the mean of the fractal

dimensions of the binary CBCTs from the people in the group $\mathcal{G}_{\mathrm{NE}}$ (non-edentulous subjects) was found to be equal to 1.61 (resp., a median of 1.61) with a standard deviation equal to 0.23 (a variance of 0.05).

Table 3. Ratio (with respect to the whole sample) and number of subjects (n) who were found some kind of septa. 74 people (18.50%) were found some type II (mediolateral vertical) or type III (anteroposterior vertical) septa.

	Type of Edentulous					
	Non-Edentulous		**Partially Edentulous**		**Totally Edentulous**	
	n	**Ratio**	***n***	**Ratio**	***n***	**Ratio**
Type II Septa	13	17.57%	35	47.30%	7	9.46%
Type III Septa	7	9.46%	8	10.81%	4	5.41%

4. Discussion

One of the main goals in this paper was to analyze the bone structure density of the trabecular tissue located in the area that surrounds the PSAA. In fact, we hypothesised that the loss of dental pieces would imply a different complexity of such a bone structure. In this way, fractal dimension plays key role since accurate calculations of such a quantity will provide us valuable information about the irregularities that the structure of that bone tissue presents at a range of scales the high resolution scanners are explored. As such, our hypothesis of study could be stated in terms of fractal dimension. Indeed, we wonder if the mean fractal dimension of the binary CBCTs of the group of edentulous patients is different from the mean fractal dimension of the binary CBCTs of the group of non-edentulous subjects. Thus, with the aim to detect some empirical evidence regarding this, it was posed the following test of hypotheses (cf. Equation (1)):

$$\begin{aligned} \mathcal{H}_0 &: \mu_{\mathrm{NE}} = \mu_{\mathrm{E}} \\ \mathcal{H}_1 &: \mu_{\mathrm{NE}} \neq \mu_{\mathrm{E}}, \end{aligned}$$

where μ_{E} denotes the mean (resp., the median) of the fractal dimensions of the binary CBCTs of the group $\mathcal{G}_{\mathrm{E}}$ (edentulous) and μ_{NE} refers to the mean (resp., the median) of the fractal dimensions of the binary CBCTs of the group $\mathcal{G}_{\mathrm{NE}}$ (non-edentulous).

Next, we comment on the sample size effects. First, from Section 3, we recall that the mean of the fractal dimensions of the binary CBCTs of the group of edentulous patients was found to be equal to 1.56 with a standard deviation of 0.12. On the other hand, a mean of 1.61 and a standard deviation equal to 0.23 were calculated in regard to the fractal dimensions of the binary CBCTs. Hence, an effect size equal to 0.27 was obtained, which according to [22] lies between a small and medium effect size. Next, we recall also that 274 CBCTs were analyzed in regard to the group of edentulous patients, whereas 126 CBCTs were assigned to the group of non-edentulous subjects. Thus, at a significance level of 0.05, a statistical power equal to 0.80 follows. Accordingly, we found that such a significance level was adequate to properly carry out that comparison.

Several statistical tests were applied at a confidence level of 95% with the aim to compare the medians (resp., the means) of the fractal dimensions of the binary CBCTs from these subgroups. It is worth mentioning that the Mann-Whitney test threw a p-value equal to 0.001 when comparing the medians of such fractal dimensions. Moreover, a p-value equal to 0.007 was provided by the Student's t-test when comparing the means of such fractal dimensions (with the hypothesis consisting of the normality of the involved samples being satisfied). These results suggest that the null hypothesis must be rejected, thus supporting our hypothesis.

In Section 3, the three quantitative variables, DME, CME, and MME were analyzed that were calculated for those CBCTs from all the patients assigned to the type I category of PSM. Interestingly, it holds that such attributes are pairwise connected by strong linear relationships.

Notwithstanding that the CBCT technology allows us to go in depth in the structure of the maxillary sinus, sometimes such based scanners may not detect the PSAA, which is present for every subject. That issue constitutes a weakness of our methodology to explore the characteristics of that artery.

5. Conclusions

In this paper, the CBCT technology, which presents a greater sensitivity and resolution capacity than a radiologic-based approach, was applied to carefully explore some anatomical features of the PSAA. In fact, several parameters were accurately measured from high quality CBCTs by Romexis 2.5.1® such as the distance from the PSAA to the bone crest, the thickness of the Schneider's membrane, and the diameter of some cavities associated to pathological membranes, to name some of them.

It becomes crucial to further analyze the bone structure density of the area that surrounds the PSAA since the posterior region of the maxillary sinus tends to lose a large amount of bone mass as a consequence of the loss of teeth, the reabsorption of the alveolar ridge, and the pneumatization process of the sinus. With this aim, the fractal dimension constitutes a valuable tool allowing to analyze the complexity of that trabecular tissue at a preoperative stage.

Our study was carried out by a sample of data from 200 participants and 400 CBCTs. Due to the large sample size, the statistical results displayed in this article constitute a useful benchmark for further research on the PSAA anatomical features and the trabecular tissue located in the area surrounding it, as well.

We found a substantial ratio of patients (the 47.30% of the partially edentulous subjects) that presented an enlargement of their Schneider's membranes, though it was not thoroughly analyzed whether there was associated any kind of pathological process. This issue and specific relationships among the presence of septa and treatment complications require further investigation.

On the other hand, it was empirically verified that the three measures calculated for those CBCTs from those patients with a pathological Schneider's membrane (distal measure, central measure, and mesial measure) are pairwise connected through strong linear relationships.

Finally, it was found statistical evidence that the fractal dimension of the trabecular tissue located in the area that surrounds the PSAA is different from the group of edentulous patients to the group of non-edentulous subjects, thus suggesting that the complexity of the trabecular tissue from each group of subjects is distinct. Our results were supported by a moderate size effect of the sample and a good statistical power.

In summary, this study highlights that a combination of the CBCT technology with accurate fractal dimension calculations do provide valuable information in regard to the area that surrounds the PSAA.

Author Contributions: Conceptualization, Y.G.-S., F.J.G.G., M.F.-M., B.P.M. and P.L.-J.; methodology, Y.G.-S., F.J.G.G., M.F.-M., B.P.M. and P.L.-J.; validation, Y.G.-S., F.J.G.G., M.F.-M., B.P.M. and P.L.-J.; formal analysis, Y.G.-S., F.J.G.G., M.F.-M., B.P.M. and P.L.-J.; writing—original draft preparation, Y.G.-S., F.J.G.G., M.F.-M., B.P.M. and P.L.-J.; writing—review and editing, Y.G.-S., F.J.G.G., M.F.-M., B.P.M. and P.L.-J.; These authors contributed equally to this work. All authors have read and agreed to the published version of the manuscript.

Funding: This research was funded by Ministerio de Ciencia, Innovación y Universidades grant number PGC2018-097198-B-I00 and by Fundación Séneca de la Región de Murcia grant number 20783/PI/18.

Acknowledgments: The authors would like also to express their gratitude to the anonymous reviewers whose suggestions, comments, and remarks have allowed them to enhance the quality of this paper.

Conflicts of Interest: The authors declare no conflict of interest.

Abbreviations

The following abbreviations are used in this manuscript:

PSAA	Posterior Superior Alveolar Artery
CBCT	Cone Beam Computed Tomography
PAA	Presence of Alveolar Artery
AAL	Alveolar Artery Location
DAB	Distance from the alveolar Artery to the Bone crest
PSM	Presence of a pathological Schneider's Membrane
DME	Distal MEasure
CME	Central MEasure
MME	Mesial MEasure
NSE	Number of SEpta
DAH	Diameter of the Anterior Hole
DPH	Diameter of the Posterior Hole

References

1. Vogiatzi, T.; Kloukos, D.; Scarfe, W.C.; Bornstein, M.M. Incidence of Anatomical Variations and Disease of the Maxillary Sinuses as Identified by Cone Beam Computed Tomography: A Systematic Review. *Int. J. Oral Maxillofac. Implants* **2014**, *29*, 1301–1314. [CrossRef]
2. De Cleyn, K.M.; Kersschot, E.A.; De Clerck, L.S.; Ortmanns, P.M.; De Schepper, A.M.; Van Bever, H.P.; Stevens, W.J. Paranasal Sinus Pathology in Allergic and Non-Allergic Respiratory Tract Diseases. *Allergy* **1986**, *41*, 313–318. [CrossRef] [PubMed]
3. Baroody, F.M.; Mucha, S.M.; deTineo, M.; Naclerio, R.M. Evidence of maxillary sinus inflammation in seasonal allergic rhinitis. *Otolaryngol. Head Neck Surg.* **2012**, *146*, 880–886. [CrossRef] [PubMed]
4. Pérez Sayáns, M.; Suárez Quintanilla, J.A.; Chamorro Petronacci, C.M.; Suárez Peñaranda, J.M.; López Jornet, P.; Gómez García, F.; Guerrero Sánchez, Y. Volumetric study of the maxillary sinus in patients with sinus pathology. *PLoS ONE* **2020**, *15*, e0234915. [CrossRef] [PubMed]
5. Kim, Y.K.; Hwang, J.Y.; Yun, P.Y. Relationship between prognosis of dental implants and maxillary sinusitis associated with the sinus elevation procedure. *Int. J. Oral Maxillofac. Implants* **2013**, *28*, 178–183. [CrossRef]
6. Wang, L.-L.; Chen, F.-J.; Yang, L.-S.; Li, J.-E. Analysis of pathogenetic process of fungal rhinosinusitis: Report of two cases. *World J. Clin. Cases* **2020**, *8*, 451–463. [CrossRef] [PubMed]
7. Friedland, B.; Metson, R. A Guide to Recognizing Maxillary Sinus Pathology and for Deciding on Further Preoperative Assessment Prior to Maxillary Sinus Augmentation. *Int. J. Periodontics Restor. Dent.* **2014**, *34*, 807–815. [CrossRef]
8. Varela-Centelles, P.; Loira-Gago, M.; Seoane-Romero, J.M.; Takkouche, B.; Monteiro, L.; Seoane, J. Detection of the posterior superior alveolar artery in the lateral sinus wall using computed tomography/cone beam computed tomography: A prevalence meta-analysis study and systematic review. *Int. J. Oral Maxillofac. Surg.* **2015**, *44*, 1405–1410. [CrossRef]
9. Park, Y.-B.; Jeon, H.-S.; Shim, J.-S.; Lee, K.-W.; Moon, H.-S. Analysis of the Anatomy of the Maxillary Sinus Septum Using 3-dimensional Computed Tomography. *J. Oral Maxillofac. Surg.* **2011**, *69*, 1070–1078. [CrossRef]
10. Pagano, S.; Moretti, M.; Marsili, R.; Ricci, A.; Barraco, G.; Cianetti, S. Evaluation of the Accuracy of Four Digital Methods by Linear and Volumetric Analysis of Dental Impressions. *Materials* **2019**, *12*, 1958. [CrossRef]
11. Rahpeyma, A.; Khajehahmadi, S. Alveolar Antral Artery: Review of Surgical Techniques Involving this Anatomic Structure. *Iran. J. Otorhinolaryngol.* **2014**, *26*, 73–78. [PubMed]
12. Fernández-Martínez, M.; Gómez García, F.J.; Guerrero-Sánchez, Y.; López Jornet, P. An intelligent system to study the fractal dimension of trabecular bones. *J. Intell. Fuzzy Syst.* **2018**, *35*, 4533–4540. [CrossRef]
13. Fernández-Martínez, M.; Guerrero-Sánchez, Y.; López-Jornet, P. A novel approach to improve the accuracy of the box dimension calculations: Applications to trabecular bone quality. *Discret. Contin. Dyn. Syst.-S* **2019**, *12*, 1527–1534. [CrossRef]

14. Ilgüy, D.; Ilgüy, M.; Dolekoglu, S.; Fisekcioglu, E. Evaluation of the Posterior Superior Alveolar Artery and the Maxillary Sinus With CBCT. *Braz. Oral Res.* **2013**, *27*, 431–437. [CrossRef] [PubMed]
15. Pandharbale, A.A.; Gadgil, R.M.; Bhoosreddy, A.R.; Kunte, V.R.; Ahire, B.S.; Shinde, M.R.; Joshi, S.S. Evaluation of the Posterior Superior Alveolar Artery Using Cone Beam Computed Tomography. *Pol. J. Radiol.* **2016**, *81*, 606–610. [CrossRef] [PubMed]
16. Khojastehpour, L.; Dehbozorgi, M.; Tabrizi, R.; Esfandnia, S. Evaluating the Anatomical Location of the Posterior Superior Alveolar Artery in Cone Beam Computed Tomography Images. *Int. J. Oral Maxillofac. Surg.* **2016**, *45*, 354–358. [CrossRef] [PubMed]
17. Velasco-Torres, M.; Padial-Molina, M.; Alarcón, J.A.; O'Valle, F.; Catena, A.; Galindo-Moreno, P. Maxillary Sinus Dimensions With Respect to the Posterior Superior Alveolar Artery Decrease With Tooth Loss. *Implant Dent.* **2016**, *25*, 464–470. [CrossRef] [PubMed]
18. Santos German, I.J.; Vieira Buchaim, D.; Andreo, J.C.; Hitoshi Shinohara, E.; Alvares Capelozza, A.L.; Shinohara, A.L.; Rosa Junior, G.M.; Pereira, M.; Buchaim, R.L. Identification of the Bony Canal of the Posterior Superior Alveolar Nerve and Artery in the Maxillary Sinus: Tomographic, Radiographic, and Macroscopic analyzes. *Sci. World J.* **2015**. [CrossRef]
19. Bornstein, M.M.; Fernández-Martínez, M.; Guirao, J.L.G.; Gómez-García, F.J.; Guerrero-Sánchez, Y.; López-Jornet, P. On the Symmetry of the Bone Structure Density over the Nasopalatine Foramen via Accurate Fractal Dimension Analysis. *Symmetry* **2019**, *11*, 202. [CrossRef]
20. Fernández-Martínez, M.; Guirao, J.L.G.; Sánchez-Granero, M.A. Calculating Hausdorff Dimension in Higher Dimensional Spaces. *Symmetry* **2019**, *11*, 564. [CrossRef]
21. Fernández-Martínez, M.; Guirao, J.L.G.; Sánchez-Granero, M.A.; Trinidad Segovia, J.E. *Fractal Dimension for Fractal Structures. With Applications to Finance*, 1st ed.; Springer Nature: Cham, Switzerland, 2019; pp. 1–204.
22. Sawilowsky, S.S. New Effect Size Rules of Thumb. *J. Mod. Appl. Stat. Methods* **2009**, *8*, 597–599. [CrossRef]